IET Generation, Transmission & Distribution

Research Article

IET Journals
The Institution of Engineering and Technology

Energy saving estimation in distribution network with smart grid-enabled CVR and solar PV inverter

ISSN 1751-8687
Received on 1st July 2017
Revised 18th October 2017
Accepted on 25th October 2017
E-First on 12th February 2018
doi: 10.1049/iet-gtd.2017.0973
www.ietdl.org

Shailendra Singh[1], Shiv P. Singh[1] ✉

[1]*Department of Electrical Engineering, Indian Institute of Technology (BHU) Varanasi, Varanasi, Uttar Pradesh, India*

✉ *E-mail: spsingh.eee@itbhu.ac.in*

Abstract: Estimation of energy savings in distribution network through smart grid-enabled conservation of voltage reduction (CVR) approach has been investigated in this study. To achieve higher-energy savings, CVR operation has been carried out with deeper voltage reduction in association with photovoltaic (PV) system while keeping the node voltages within acceptable limits. The additional reactive power support has been injected by PV inverters. The injected reactive power has been controlled by droop characteristics method. Besides, the moving cloud transient effect has been incorporated in PV power output. To evaluate the energy savings, the volt-VAR control operation has been carried out in three different modes such as without CVR, only CVR, and CVR with PV system on the modified unbalanced IEEE 123 node test system. The test system and control algorithms have been developed and simulated in open distribution system simulator interfaced with MATLAB. From simulation results, it has been demonstrated that higher-energy savings and peak load demand reduction can be achieved through smart grid-enabled CVR and PV system in comparison with the only CVR with proper voltage regulation.

Nomenclature

Tap	tap position of OLTC transformer/AVRs
V_{reg}	voltage at regulation point
E_{Saving}	energy savings
$E_{\text{no-CVR}}$	energy consumption during normal or no-CVR operation
E_{CVR}	energy consumption during smart grid-enabled CVR operation
$\text{CVR}_{f_{\text{E}}}$	CVR factor in kWh
ΔV_{tr}	variation in voltage per step of OLTC/AVR which is specified by the manufacturer
Δq^{i}_{cb}	per step variation in reactive power at the ith CB
$\text{Sw}^{i}_{\text{cb}}$	switching step number of the ith CB
Q^{i}_{cb}	reactive power injected by an ith CB
$\text{Sw}^{i,\text{max}}_{\text{cb}}$	maximum number of switching steps available at the ith CB
P^{inv}_{T}	actual real power output from inverter at time T
Q^{inv}_{T}	actual reactive power output from inverter at time T
P_{T}	active power generated by PV arrays at time T
Q_{T}	actual reactive power output at time T
$P^{\text{Inv}}_{T,\text{loss}}$	active power inverter loss at time T
S_{max}	maximum apparent power rating of the inverter
$Q^{\text{inv,max}}_{T}$	available maximum reactive power capacity
η_{inv}	inverter efficiency
P_{Demand}	total real power demand at substation
P_{load}	total active power load demand
P_{loss}	total real power losses
$P_{\text{L},k}(V_k)$	active power load at the kth node expressed as function of V_k
$Q_{\text{L},k}(V_k)$	reactive power load at the kth node expressed as a function of V_k
nl	number of load buses (node)
V_k	voltage at the kth node
V_{p}	primary side voltage of OLTC/AVR
V_{tr}	regulated voltage at secondary side of OLTC/AVR
V_{base} or V_n	base voltage or nominal voltage
a, b, c	phase(Φ) a, b, and c
$N^{i}_{\text{tr},h}$	total tap change of the ith (OLTC/AVR) device at the hth hour
$N^{i}_{\text{tr,max}}$	maximum number of daily tap change of the ith (OLTC/AVR) device
$N^{i}_{\text{sw},h}$	total switching operation of the ith CB device at the hth hour
CT_{p}	primary current in current transformer (CT)
CT_{s}	secondary current in CT
CT_{ratio}	CT ratio
$V_{\text{LN,rated}}$	rated line to neutral voltage
$\text{KVA}^{\text{Trf}}_{\text{rated}}$	KVA rating of transformer
$\text{KV}^{\text{Trf}}_{\text{rated}}$	rated KV voltage of transformer
V_{LN}	line to neutral voltage
$N^{i}_{\text{sw,max}}$	maximum number of daily switching operation of the ith CB device
$V^{\text{mon}}_{i,T}$	monitored line voltage at the ith line at time T
$Q^{\text{mon}}_{i,T}$	monitored line reactive power flow at the ith line at time T
$Q^{\text{min}}_{i,T}$	minimum reactive power flow limit of the ith line at time T
$Q^{\text{max}}_{i,T}$	maximum reactive power flow limit of the ith line at time T

1 Introduction

The conventional distribution systems (DSs) are facing numerous technical, industrial, and economic issues, since past few decades due to fast variations in power demand and a shift in energy paradigm [1]. Conservation of voltage reduction (CVR) reduces the voltage willingly in such a manner that it neither violates the American National Standards Institute (ANSI) Standard C84 limits [2] nor affects the performance of customer devices. It is enabled through the advance functioning of integrated volt-VAR (VV) control (VVC) mechanism. To reduce the peak load demand and energy consumption, various power utilities have already applied CVR technology as reported in [3]. However, its implementation, assessment, and power quality issues pose three technical barriers such as:(i) optimal coordination among VV regulatory devices; (ii) appropriate assessment and verification of CVR effects; and (iii) coordination between CVR and distributed energy resource (DER) as mentioned in [3]. Recently, higher-energy saving through CVR

has been achieved in many countries [4–6]. Field trial-based implementation of CVR has been reported in [4–7]. Enabling of CVR has been achieved with the VV field devices through CVR voltage settings [4]. Network sensitivity-based method for voltage reduction has been utilised in [5]. Deployment of CVR in [6] has been achieved by reactive power control through capacitors and voltage optimisation. In [7], the voltage reduction up to 4% in the meshed network has been successfully implemented using load tap changer with the use of line drop compensation (LDC) scheme. A closed-loop distribution management system (DMS)-based VVC through LDC approach has been implemented in smart grid environments [8]. A VV optimisation method with the multi-objectives of minimising total demand and node voltage deviation has been presented in [9]. The work reported in [4–9] is restricted to voltage reduction range and has been implemented with the help of conventional VV devices. Moreover, the effect of additional power devices has not been analysed. Effect of capacitors as an additional reactive power support during deeper voltage reduction has been analysed in [10, 11].

Most of the above-reported work deals with the first and second technical barriers of CVR. Few research works relevant to third technical barrier are reported in the literature. Simplified sensitivity-based approach for voltage control with the coordination of VV regulation device and distributed generation (DG) has been carried out in [12]. Bokhari *et al.* [13] and Quijano and Feltrin [14] have analysed the combined impact of CVR and DG. Mitigation of low-voltage violation during deeper voltage reduction is achieved with DG penetration in [13]. Multi-objective VV optimisation-based method has been proposed to assess the CVR effect with various levels of DG penetration in [14]. However, it is difficult for the operator to choose an appropriate set of VVC settings from multi-objective solutions. In [15], the effect of photovoltaic (PV) DER penetrations during CVR is investigated with various cases of VVC, but the ability of PV inverter is not fully utilised. The work presented by above authors may be useful for CVR study. However, it lacks the cooperation of the distributed renewable sources due to intermittent behaviour and slow operation of traditional VV controlling devices.

The impact of PV inverters as VAR support and voltage regulation device has been analysed in [16–23]. For full utilisation of PV park, the voltage modulation-based method for reactive energy compensation through PV inverter is presented in [16]. However, this method is tested for prototype model without proper control mechanism. Decentralised voltage control through PV generator with reactive power support is presented in [17, 18]. The objective of minimising the voltage deviation between control and reference buses is accomplished through Lyapunov theory in [17]. Using this method, it is not easy to identify the best control bus in the partitioned network; hence, solution may trap in local minima. In [18], the voltage sensitivity and droop control-based approach have been used to calculate the voltage deviation and power flow control. Jahangiri and Dionysios [19], Juamperez and Guangya [20], and Smith *et al.* in [21] have analysed the impact of PV inverters for over voltage problem with VV droop control scheme. The optimal power support for voltage control through distributed energy storage system for clustered network has been discussed in [22]. A voltage sensitivity-based control method with the objective of minimising reactive power flow and total active power losses through inverter-type DG is presented in [23]. However, authors in [16–23] have not analysed the voltage control through PV inverter during CVR. Combined effect of CVR and PV inverters has been demonstrated in [24–27]. In [24], a slow and fast time-scale-based VVC scheme for CVR is proposed with the objective of minimising total energy consumption. However, the effect of voltage-dependent load model is not considered in this paper. The optimal reactive power support through PV inverter with the objective of minimising voltage deviation has been presented in [25]. Significant energy savings have been reported in [26] through CVR with reactive power compensation. Although, compensated reactive power from the DG inverter has not been controlled in this paper. The closed-loop CVR problem has been analysed through reactive power support from PV inverter in [27]. However, this method has been tested only for limited voltage reduction range on the simple-balanced network considering impedance load model.

An attempt has been made in this investigation to address the second and third technical barriers for which a smart grid-enabled CVR scheme for VVC has been proposed. To control the tap position of on-load tap changer (OLTC)/automatic voltage regulator (AVR), a well-established LDC scheme has been employed in this paper. The limits of tap change and capacitor bank (CB) switching for daily operation have been considered in control algorithms. Besides, CVR in association with PV system has been implemented to achieve a greater saving in peak demand and energy consumption even during deeper voltage reduction. In addition, reactive power compensation is done through PV inverters to control the lower-voltage violation. The desired reactive power is calculated and controlled through VV droop control mechanism. The effect of inverter losses due to reactive current generation during reactive power support has also been included. The moving cloud transient effect has been considered while developing the solar PV model. The proposed scheme has been tested on unbalanced radial distribution network with voltage-dependent composite ZIP load models for peak demand hours and whole day operation. The effect of various types of loadings such as residential, commercial and industrial are also incorporated in the load model.

2 Smart grid-enabled CVR

The basic aim of CVR technology is the conservation of energy by marginal reduction in voltage (normally 2–6% of nominal value) at user end nodes. Thus, by setting the regulation voltage in ANSI lower half (114–120 V) range, saving in energy can be achieved. However, while reducing the voltage, CVR should meet the International Standards ANSI C84.1–2006 [2]. Application of CVR with traditional schemes has not been found much effective, because of restricted voltage reduction range, inaccurate load modelling and the unavailability of end user information. To overcome the above barriers and achieve higher-energy savings, a smart grid-enabled CVR approach has been presented in this paper. The operation of CVR through VVC approach is carried out by enabling of smart grid assets in local as well as the global domain of the distribution network.

The schematic diagram of integrated VVC with CVR for a distribution network has been shown in Fig. 1. To achieve the maximum energy savings, VVC server calculates the controlled parameters of different field assets with the coordination of CVR server and advanced DMS. The field devices are connected to the servers through communication links. Advanced DMS regularly monitors and evaluates the power and voltage profile, throughout the distribution network with the help of advanced metering infrastructure (AMI) systems. The proposed scheme first accumulates the measurements and then generates proper control signals. These control signals are transmitted through suitable communication links to VVC field devices. Accurate loads are derived through AMI data which plays the prime role in enabling the CVR scheme in planning or in real-time framework.

Assessment of CVR effects is judged through the CVR factor. Mathematically in terms of energy (CVR_{fE}), it is calculated as the ratio of the total E_{Saving} in percentage, and amount of voltage reduction (ΔV) over a time horizon in percentage as articulated in (1) and (2)

$$E_{\mathrm{Saving}} = \left(\frac{E_{\mathrm{no-CVR}} - E_{\mathrm{CVR}}}{E_{\mathrm{no-CVR}}} \right) \tag{1}$$

$$\mathrm{CVR}_{fE} = \frac{(E_{\mathrm{saving}})\%}{\Delta V\%} \tag{2}$$

3 System components modelling

A DS is the combination of one or more distribution feeders, which supply the electricity to the consumers end. The components of distribution feeder can be classified as series and shunt feeder components. Series feeder components are line segments, voltage

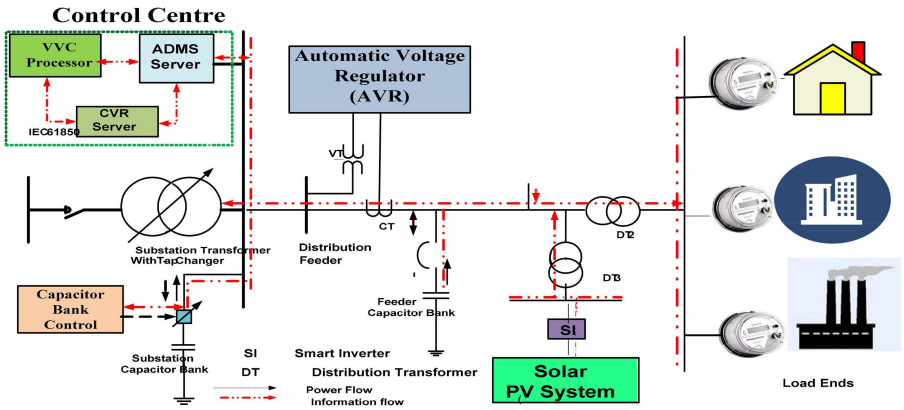

Fig. 1 *Substation-based smart grid-enabled CVR*

regulators and transformers, whereas spot and distributed loads and capacitor banks are generally termed as shunt components. Accurate modelling of both series and shunt components is necessary for close observation of distribution feeder. Models of these components used in this study have been described in further sections.

3.1 Line segment model

An exact line segment model is considered in this paper. Voltage and current relations for exact line segment model with respect to input node 'h' and output node 'k' can be expressed as given below [28]:

$$[\mathrm{VLG}_{\mathrm{abc}}]_h = [\boldsymbol{a}] \cdot [\mathrm{VLG}_{\mathrm{abc}}]_k + [\boldsymbol{b}] \cdot [I_{\mathrm{abc}}]_k \tag{3}$$

where

$$[\boldsymbol{a}] = [u] + \frac{1}{2}[Z_{\mathrm{abc}}] \cdot [Y_{\mathrm{abc}}] \tag{4}$$

$$[\boldsymbol{b}] = [Z_{\mathrm{abc}}] \tag{5}$$

and $[\boldsymbol{u}]$ is the identity matrix

$$[\mathrm{VLG}_{\mathrm{abc}}]_k = [\boldsymbol{a}]^{-1} \cdot ([\mathrm{VLG}_{\mathrm{abc}}]_h - [\boldsymbol{b}] \cdot [I_{\mathrm{abc}}]_k) \tag{6}$$

$$[I_{\mathrm{abc}}]_h = [\boldsymbol{c}] \cdot [\mathrm{VLG}_{\mathrm{abc}}]_k + [\boldsymbol{d}] \cdot [I_{\mathrm{abc}}]_k \tag{7}$$

$$[\boldsymbol{c}] = [Y_{\mathrm{abc}}] + \frac{1}{4} \cdot [Y_{\mathrm{abc}}] \cdot [Z_{\mathrm{abc}}] \cdot [Y_{\mathrm{abc}}] \tag{8}$$

$$[\boldsymbol{d}] = [\boldsymbol{u}] + \frac{1}{2}[Z_{\mathrm{abc}}] \cdot [Y_{\mathrm{abc}}] \tag{9}$$

Equations (3) and (7) can be rearranged in (10) to yield

$$\begin{bmatrix} [\mathrm{VLG}_{\mathrm{abc}}]_h \\ [I_{\mathrm{abc}}]_h \end{bmatrix} = \begin{bmatrix} \boldsymbol{a} & \boldsymbol{b} \\ \boldsymbol{c} & \boldsymbol{d} \end{bmatrix} \begin{bmatrix} [\mathrm{VLG}_{\mathrm{abc}}]_k \\ [I_{\mathrm{abc}}]_k \end{bmatrix} \tag{10}$$

where Z_{abc} and Y_{abc} are the impedance and shunt admittance of the line segment. $[\mathbf{VLG}_{\mathrm{abc}}]_h$ and $[\mathbf{VLG}_{\mathrm{abc}}]_k$ are the line-to-ground voltage matrixes at node h and k, respectively. $[\boldsymbol{I}_{\mathrm{abc}}]_h$ and $[\boldsymbol{I}_{\mathrm{abc}}]_k$ are the node current matrixes at node 'h' and 'k', respectively. The value of shunt admittance is, in general, very small. Therefore, it can be neglected for simplification of the network. Similarly, voltage and current equations can be obtained for other series components. The generalised equations for series components can be written in the following equations (11) and (12):

$$[\mathbf{VLG}_{\mathrm{abc}}]_k = [\boldsymbol{A}][\mathbf{VLG}_{\mathrm{abc}}]_h - [\boldsymbol{B}][\boldsymbol{I}_{\mathrm{abc}}]_k \tag{11}$$

$$[\boldsymbol{I}_{\mathrm{abc}}]_h = [\boldsymbol{C}] \cdot [\mathbf{VLG}_{\mathrm{abc}}]_k + [\boldsymbol{D}] \cdot [\boldsymbol{I}_{\mathrm{abc}}]_k \tag{12}$$

The values of matrices $[\boldsymbol{A}]$, $[\boldsymbol{B}]$, $[\boldsymbol{C}]$, and $[\boldsymbol{D}]$ will change according to the series components. Detail modelling of these series and shunt components is well documented in [28].

3.2 Voltage control devices

Voltage regulating devices are widely used for not only maintaining the acceptable voltage profile throughout the network, but they also play a crucial role in the healthy operation of the distribution grids. Voltage regulators, OLTC transformers, and capacitor banks are the most commonly used voltage regulating devices. With advancement in smart grid technologies, grid-connected power sources such as solar PV with smart inverters also provide voltage support to the system as voltage regulating devices [24].

3.2.1 OLTC transformer and AVR: An OLTC transformer is used to vary the voltage across the network. It is generally located at the source substation side. The provision of tap changing is made toward high-voltage side in off-load changing transformers, whereas tap-changing mechanism is provided toward low-voltage side in OLTC. It can be represented as the simple circuitry of an ideal transformer with series branch admittance as described in [27, 29]. The OLTC transformer's tap position and its transformation ratio (a_{tr}) can be utilised to determine the voltage variation as expressed by (13)

$$a_{\mathrm{tr}} = 1 \pm \left(\frac{\Delta V_{\mathrm{tr}}}{100}\right) \times \mathrm{Tap} \tag{13}$$

In (13), the minus/plus sign is used to denote the raise/lower in the tap position.

AVR is formed by combining an autotransformer and load tap-changing mechanism. It is located at the source end and/or downstream of the feeder. It can be modelled as a tap-changing autotransformer with very small series impedance and shunt admittance. The AVR with taps in the series winding side is considered type A and that having taps on the source side is called type B. Type B is widely used for downstream feeders for which the voltage regulation is governed by (13).

3.2.2 Capacitor banks: Capacitor banks are a group of fixed and switchable shunt capacitors. CBs should be equipped with controllers (in the case of switchable shunt capacitors) in order to regulate voltage and reactive power flows efficiently. Reactive power supplied by CB at each switching operation is determined using (14)

$$Q_{\mathrm{cb}}^{i} = \mathrm{Sw}_{\mathrm{cb}}^{i} \Delta q_{\mathrm{cb}}^{i}, \ \mathrm{Sw}_{\mathrm{cb}}^{i} = \left\{0, 1, 2, \ldots, \mathrm{Sw}_{\mathrm{cb}}^{i,\max}\right\} \tag{14}$$

3.2.3 Solar PV inverter: Apart from the basic inversion function, modern PV inverters have many advance attractive features. They have the capability to inject or consume the reactive power from the grid and operate as distributed VVC device. In addition, PV

inverters contribute significantly to the improvement of distribution network operation by maintaining the voltage profile and losses reduction**.** However, it may cause some additional loss while performing reactive power support function.

The actual real and reactive power output from inverter (P_T^{inv}, Q_T^{inv}) including the inverter losses are determined by the following equations at given time T:

$$P_T^{\text{inv}} = P_T - P_{T,\text{loss}}^{\text{inv}} \tag{15}$$

$$Q_T^{\text{inv}} \simeq Q_T \tag{16}$$

$$P_{T,\text{loss}}^{\text{Inv}} = (1 - \eta_{\text{inv}}) \cdot \left(\sqrt{P_T^2 + Q_T^2}\right) \tag{17}$$

The available $Q_T^{\text{inv, max}}$ is dependent on the real power generation for a period T which is governed by (18) as applied in [19, 27]

$$|Q_T^{\text{inv, max}}| = \sqrt{S_{\max}^2 - P_T^2} \tag{18}$$

On the basis of P_T and $S_{\max}$, $Q_T^{\text{inv, max}}$ is recalculated at every time period, T.

3.3 Voltage-dependent load model

A voltage-dependent ZIP load model is the composition of constant impedance, constant current, and constant power load model. Composite ZIP load models for active and reactive powers at point of interest have been shown by (19) and (20)

$$P_{\text{L},k}(V_k) = \left[Z_P \cdot \left(\frac{V_k}{V_n}\right)^2 + I_P \cdot \left(\frac{V_k}{V_n}\right) + P_P\right] \cdot P_{n,k} \tag{19}$$

$$Q_{\text{L},k}(V_k) = \left[Z_q \cdot \left(\frac{V_k}{V_n}\right)^2 + I_q \cdot \left(\frac{V_k}{V_n}\right) + P_q\right] \cdot Q_{n,k} \tag{20}$$

$$Z_P + I_P + P_P = 1 \tag{21}$$

$$Z_q + I_q + P_q = 1 \tag{22}$$

where in (19) and (20) Z_p, I_p, P_p and Z_q, I_q, P_q are the constant parameters of impedance, current, and power for real and reactive powers satisfying (21) and (22), respectively. $P_{n,k}$ and $Q_{n,k}$ are the base powers at nominal voltage or V_{base} at the kth node.

4 Mathematical formulation and control methodology

The basic objective of this investigation is to save energy in distribution networks. This objective can be fulfilled by reducing the demand of the system by lowering the voltage of the network. Energy savings by reducing the voltage is an advance attribute of the integrated VVC mechanism. Therefore, in this section mathematical formulation and control approach to enable the CVR through VVC is delineated as under.

4.1 Mathematical formulation

The power demand at the source substation is the sum of total real power loads and the real power losses on lines/cables ($P_{\text{loss}}^{\text{lines/cables}}$), transformers ($P_{\text{loss}}^{\text{transformers}}$), and inverters ($P_{\text{loss}}^{\text{inverter}}$) as expressed by (23)–(25)

$$P_{\text{Demand}} = \sum (P_{\text{load}} + P_{\text{loss}}) \tag{23}$$

where

$$P_{\text{load}} = \sum_{\phi \in a,\, b,\, c} \sum_{k=1}^{nl} (P_{\text{L},k}(V_k))_\phi \tag{24}$$

and

$$P_{\text{loss}} = \sum \left(P_{\text{loss}}^{\text{lines/cables}} + P_{\text{loss}}^{\text{transformers}} + P_{\text{loss}}^{\text{inverter}}\right) \tag{25}$$

From (24), it can be observed that the real power demand at a node is dependent on its voltage. Furthermore, (19) reveals that the demand would decrease with a decrease in voltage. Transformer core losses depend on voltage, whereas transformer winding and line losses mainly depend on current flows. Inverter losses take place due to electronic circuitry and flow of reactive current when PV inverter absorbs/inject the reactive power. Therefore, total active power losses may decrease or increase with reduced voltage. Moreover, it also depends on several other factors such as network topology, load models, and load types.

The reduction of voltage is obtained through manoeuvring the tap position of OLTC transformer and AVRs. Equations (26) and (27) express the regulated output voltage from OLTC/AVR

$$V_{\text{tr}} = a_{\text{tr}}\, V_P \tag{26}$$

$$V_{\text{tr}} = \left\{1 \pm \left(\frac{\Delta V_{\text{tr}}}{100}\right) \times \text{Tap}\right\} \times V_P \tag{27}$$

Daily tap operation of OLTC/AVR is governed by (28) to prevent the degradation of the life cycle of voltage regulation devices

$$\sum_{h=1}^{24} N_{\text{tr},h}^i \le N_{\text{tr, max}}^i \tag{28}$$

Reactive power supplied by CBs at each switching operation is defined by (14) and daily switching operation of CBs should follow the relation (29):

$$\sum_{h=1}^{24} N_{\text{sw},h}^i \le N_{\text{sw, max}}^i \tag{29}$$

Reactive power compensation from PV inverter is determined by advance VV droop characteristics as shown in Fig. 2*a*. These characteristics can further be expressed as relation (30)

$$Q_T^{\text{inv}}(V) = \begin{cases} Q_T^{\text{inv, max}} & V < V_1^{P_1} \\ \dfrac{V - V_1^{P_1}}{V_1^{P_1} - V_2^{P_2}} Q_T^{\text{inv, max}}, & V_1^{P_1} \le V < V_2^{P_2} \\ 0 & V_2^{P_2} \le V \le V_3^{P_3} \\ -\dfrac{V - V_3^{P_3}}{V_4^{P_4} - V_3^{P_3}} Q_{T,}^{\text{inv, max}} & V_3^{P_3} < V \le V_4^{P_4} \\ -Q_T^{\text{inv,max}} & V > V_4^{P_4} \end{cases} \tag{30}$$

where $Q_T^{\text{inv, max}}$ is governed by (18).

According to ANSI, the node voltage magnitude limit is defined by the following equation:

$$V_{i,T}^{\min} \le V_{i,T} \le V_{i,T}^{\max} \quad \text{or} \quad 0.95\,\text{pu} \le V_{i,T} \le 1.05\,\text{pu} \tag{31}$$

4.2 Control methodology

Voltage and reactive power flow in the network are governed by controlling of OLTC/regulator, CB bank, and inverter. The functional control of these devices is described in this section.

4.2.1 OLTC/regulator control: LDC scheme has been adopted in this investigation to control the OLTC/regulator. The control circuitry of AVR is governed by LDC to regulate the tap position of OLTC. Fig. 2*b* shows the schematic diagram of LDC model, which consists of compensation circuit, voltage relay, and OLTC movement mechanism. The compensation circuit has a current transformer (CT), potential transformer (PT), and impedance

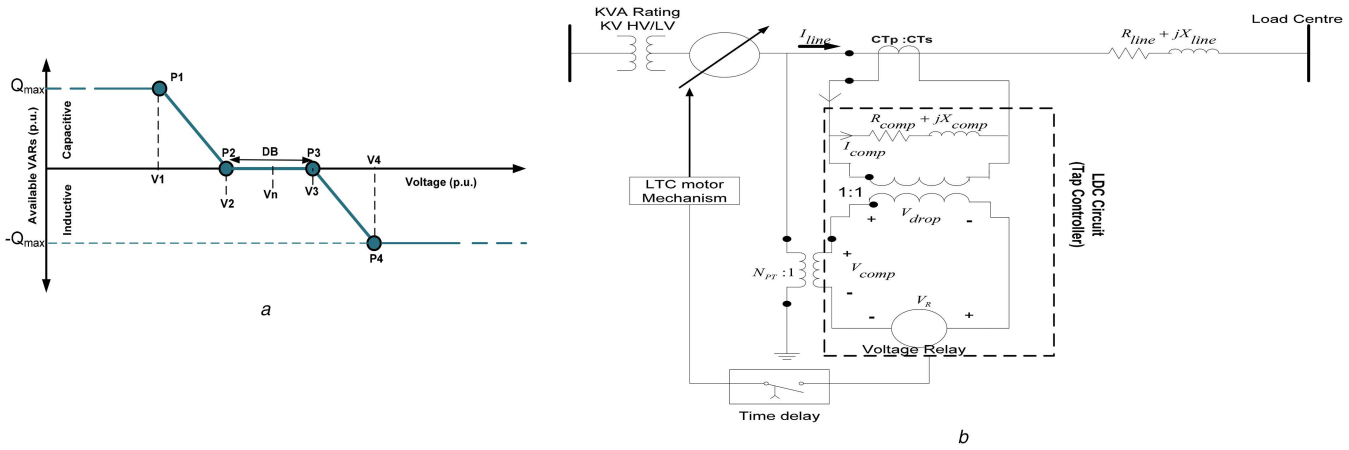

Fig. 2 *Reactive power compensation from PV inverter and OLTC/AVR control circuit*
(a) VV droop characteristics, ***(b)*** LDC model with control mechanism

If $V_{i,T}^{mon} < V_{i,T}^{\min}$

CB module is switched ON,

else if, $V_{i,T}^{mon} > V_{i,T}^{\max}$

CB module is switched OFF.

else if, $V_{i,T}^{\min} \le V_{i,T}^{mon} \le V_{i,T}^{\max}$

check the Q limits

if, $Q_{i,T}^{mon} < Q_{i,T}^{\min}$

CB module is switched ON,

else, $Q_{i,T}^{mon} > Q_{i,T}^{\max}$

CB module is switched OFF.

end

end

Fig. 3 *Capacitor bank control*

matching transformer with R & X setting. These settings of compensation circuit are very critical for voltage regulation because it reveals when tap change is required. In this work, the R & X settings are referred as R_{comp}, X_{comp} which represent the equivalent impedance from the regulator location to the regulation point.

To calculate the required tap following steps are executed by LDC algorithms:

- Determine the R_{comp}, X_{comp} value in ohm and volts using the following (32) and (33), respectively:

$$R_{\text{comp}} + \text{j}X_{\text{comp}} = (R_{\text{line}} + \text{j}X_{\text{line}}) \cdot \frac{\text{CT}_p}{N_{\text{PT}} \cdot \text{CT}_s} \tag{32}$$

$$R_{\text{comp}} + \text{j}X_{\text{comp}} = (R_{\text{line}} + \text{j}X_{\text{line}}) \cdot \frac{\text{CT}_p}{N_{\text{PT}}} \tag{33}$$

where R_{line} and X_{line} are the resistance and reactance of the line, respectively, and N_{PT} is the PT ratio determined by (34)

$$N_{\text{PT}} = \frac{V_{\text{LN, rated}}}{V_{\text{Base}}} \tag{34}$$

- Calculate the actual (feeder) line current (I_{line}) with the help of (35)

$$I_{\text{line}} = \left(\frac{\text{KVA}_{\text{rated}}^{\text{Trf}}}{\sqrt{3} \times \text{KV}_{\text{rated}}^{\text{Trf}}}\right) \tag{35}$$

- Find the compensator current (I_{comp}) through (36)

$$I_{\text{comp}} = \left(\frac{I_{\text{line}}}{\text{CT}_{\text{ratio}}}\right) \tag{36}$$

- Compute input voltage to the compensator circuit or compensator voltage (V_{comp}) by (37)

$$V_{\text{comp}} = \left(\frac{V_{\text{LN}}}{N_{\text{PT}}}\right) \tag{37}$$

Voltage drop (V_{drop}) in compensation circuit is determined through (38)

$$V_{\text{drop}} = (R_{\text{comp}} + \text{j}X_{\text{comp}}) \times I_{\text{comp}} \tag{38}$$

- Calculate the voltage across the voltage relay (V_{R}) using (39) which represents the voltage at regulation point

$$V_{\text{R}} = V_{\text{comp}} - V_{\text{drop}} \tag{39}$$

- If V_{R} is outside the bandwidth of regulator, then required tap change is calculated by (40). Otherwise, there is no need to change the tap position

$$\text{Tap} = \frac{(V_{\text{reg}} \pm 1 - V_{\text{R}})}{(\Delta V_{\text{r}} \times V_{\text{base}})} \tag{40}$$

V_{reg} is the regulation voltage at regulating position (set point), where $[V_{\text{reg}} \pm 1]$ is the acceptable range of end of line (EOL)/V_{reg} of the distribution feeder.

- After calculating tap value, voltage relay sends the signal to OLTC motor mechanism to change the tap position.

4.2.2 Capacitor bank control: CB control is very helpful to maintain the feeder voltage profile and reduce the system losses. This controller is supplemented with monitoring devices such as CTs, PTs, and local decision processor with connector/discounter situated at the load side of the bus. Controller device takes samples of voltage and current through CTs and PTs at the monitored location. After that, a decision is taken regarding the amount of compensation required based on control criteria such as KVAR and voltage at monitored point/devices. To control the voltage profile and reactive power flow at monitored point/device, following steps are adopted to CB control as delineated under (Fig. 3).

The specified value of $Q_{i,T}^{\min}$ is 40% of the rating of CBs and $Q_{i,T}^{\max}$ is 60% of the rating of CBs in the reverse direction.

4.2.3 PV inverter control: In this paper, inverter control circuitry deals mainly with calculation of the desired reactive power at each

time period T. To determine it, a droop characteristics based scheme has been utilised. The VV droop characteristics is shown in Fig. 2*a*. It is piecewise linear to the voltage and also changes dynamically due to dependency on the $Q_T^{\text{inv, max}}$. The droop characteristics are obtained by defining the four points (P_1, P_2, P_3, and P_4) parameters and dead band (DB). The DB is defined as the width between points P_2 and P_3 in terms of voltage range symmetrical to V_n. The inverter in DB range neither absorbs nor injects the VAR. Below the point P_2 ($V_2^{P_2}$), inverter starts injecting reactive power to the grid. However, when a voltage is above point P_3 ($V_3^{P_3}$), inverter absorbs reactive power from the grid. The amount of reactive power injected/absorbed by the inverter is determined using (30).

5 Implementation of VVC scheme

The control approach for various controllers is well explained earlier in Section 4. To estimate the energy savings and CVR factor, VVC is carried out in three different modes with developed controllers as delineated under.

5.1 Mode 1 (without CVR or normal operation)

In this mode, VVC operation is performed within the upper range of the service voltage known as normal, i.e. no- CVR operation. EOL/regulated voltages in regulator control is set between 121 and 126 V with V_{base} of 120 V. Shunt capacitors of CB are fixed in nature. Only LTC/regulator controllers are active in this mode.

5.2 Mode 2 (only CVR)

In this mode, VVC operation is carried out with only CVR scheme without any additional power support. CVR scheme is enabled through LDC with the setting of regulated/EOL voltages in the lower half range (114–119 V) of the service voltage. CBs are switchable in this mode. Only inverter controller is inactive in this mode. The level of voltage reduction is increased to achieve higher-energy savings with only CVR mode. However, this may lead to violation of the minimum voltage limits at some points of the distribution feeder.

5.3 Mode 3 (CVR with PV)

To achieve higher-energy saving through deeper CVR and maintain the minimum allowable voltage throughout the feeder length, an additional power source is required. Therefore, in this mode, CVR is enabled with additional power support from PV system. The required additional active/reactive power is provided through PV system with the advance functioning of solar PV inverter. The cloud transient effect is considered in PV power output.

The implementation of three modes has been done in three stages as shown in Fig. 4 and explained as under:

(I). The first stage deals with the development of the network model of considered test system including controllers. After that, the VVC operation mode is selected from the control panel and the required parameters such as EOL/V_{reg} are set. The controllers for selected mode are enabled.

(II). The second stage is mainly based on execution of control actions, power flow analysis, and verification of solution limits. Control actions execution for enabled controllers can be set either simultaneously or with some delayed action. The stepwise procedure of this stage is delineated under:

- Sample the control elements inputs.
- Set the controllers ON/OFF time delay, if delay in control queuing is enabled.
- Determine governing VVC parameters using control algorithms.
- Calculate required tap settings for OLTC/AVR through LDC using (40).
- Perform ladder iterative method for load flow analysis and obtain the feasible solution.
- Find CB switching step and reactive power support from inverter using (14) and (30), respectively.
- If control action is completed, then verify the violation limits else again execute control action.
- If obtained results are within limits, then accept the solution and store the data, if not, go to the selection of VVC mode of operation.

(III). In the third stage, estimation of energy savings and CVR factor is performed through data obtained using (1) and (2), respectively.

6 Simulation results and discussion

In this section, the simulation results of test cases have been presented and discussed. For the assessment of CVR effect, a modified IEEE 123 node distribution test feeder [30] has been considered as shown in Fig. 5*a*. Ratings and parameters of VVC devices have been shown in Table 1. Modelling of the distribution network, controllers, PV system, and power flow calculations have been done and simulated on open DS simulator (OpenDSS) platform [31]. However, the control algorithms have been written in MATLAB and interfaced with OpenDSS. Before performing simulations of the test systems, following assumptions have been incorporated:

- The communication system is working well, and its delay effect has been ignored during the execution of CVR.
- Data upgradation duration of 15 min has been taken for AMI system and field devices.
- ZIP load models are considered throughout the distribution network with and without CVR operations. ZIP coefficients are depicted in Table 2.
- Load allocation factor for distributed load is set to 1 in OpenDSS inbuilt allocation algorithm.
- Load demand profile with active and reactive power demand multipliers for 24 h with 15 min interval of a typical day has been considered, and it is shown in Fig. 5*b*.
- The switching effect is neglected during the operation of switched shunt capacitor banks. However, switching time has been incorporated taking a suitable time delay in control queuing.

The test system has been simulated for two cases to analyse the CVR effects explained below.

6.1 Case I – peak demand reduction

Peak demand reduction through CVR is investigated in this case study. The demand above 95% of the highest active power demand has been considered as the peak demand hours in the present study. The duration of such load on the test system under consideration spreads from 14:15 to 19:00 h which approximates to 5 h. The load profile of a typical day is shown in Fig. 5*b* along with peak demand hours. The effect of CVR on peak demand reduction in three modes of VVC operation has been analysed under this loading condition.

6.1.1 Mode 1: The simulation results for the peak demand duration without CVR (normal operation) have been obtained with the application of VVC to maintain 124 V regulated voltage/EOL with the help of LDC settings. The results of this mode of operation are shown in the second column of Table 3. The active power demand of the system is shown in Fig. 6*a* for considered duration.

6.1.2 Mode 2: The test system, for this mode of operation, has been simulated for two different regulated voltages of 119 and 117 V. The results have been given in the third column of Table 3. From results, it can be observed that a significant reduction in energy demand about 1.96 and 2.81% is achieved at 119 and 117 V, respectively, in comparison with Mode 1. However, the energy

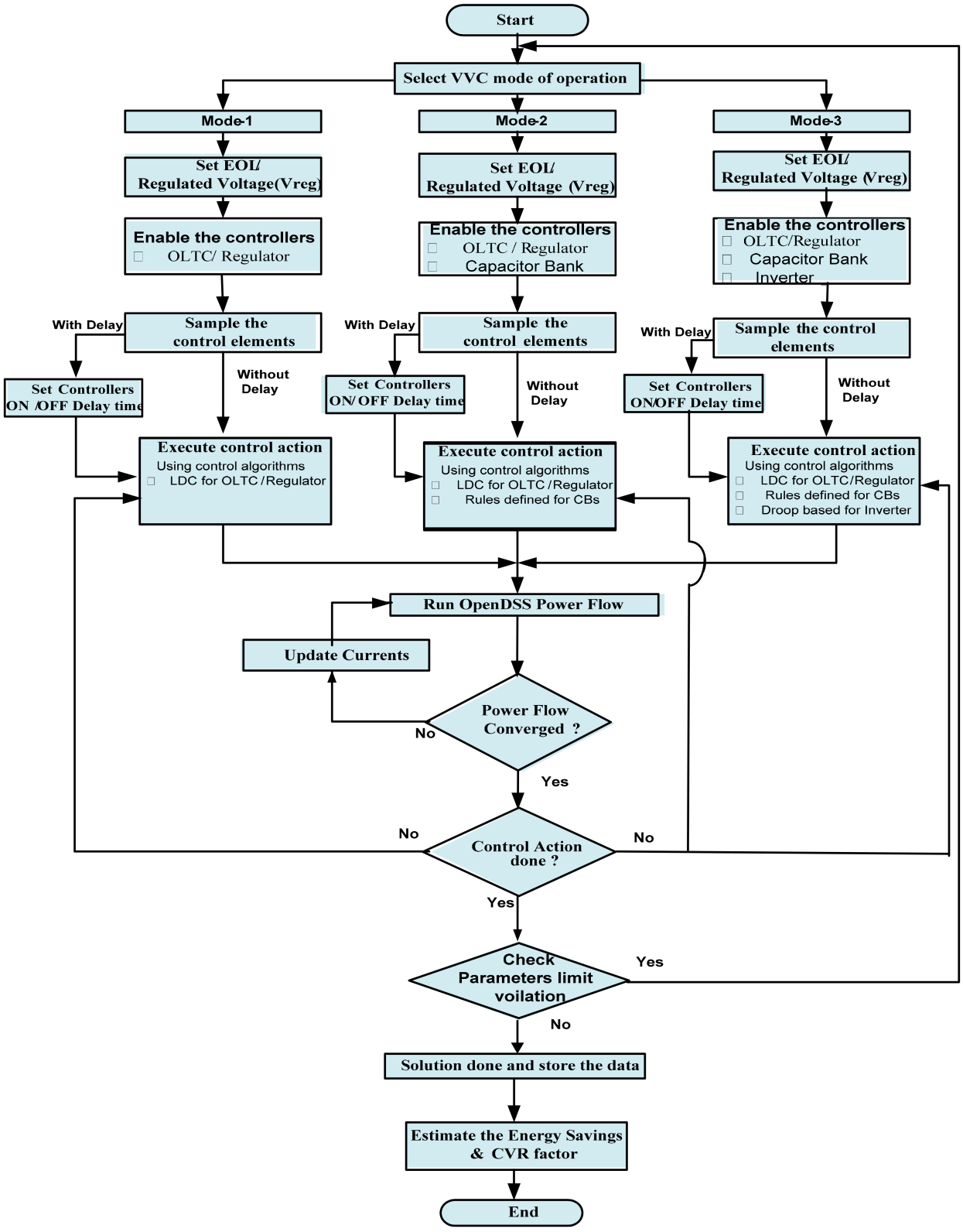

Fig. 4 *Flowchart of VVC mode of operation*

losses have been slightly (about 3.2% for 119 V and 4.7% for 117 V) increased. The increased losses are not so significant and can be overlooked because reductions in energy consumptions are sufficiently higher than the increased energy losses. From Fig. 6*b*, it is further observed that there are no violations of minimum voltage limit (below 0.95 pu) at 119 V. However, during deeper voltage reduction (CVR at 117 V regulated voltage) the minimum voltage limits have been violated. The maximum voltage deviation from permissible voltage (0.95 pu) is 0.006 pu. The lowest voltage of 0.944 pu has been observed at node 65. Fig. 6*a* shows the total active power demanded from the substation. The CVR_{fE} is 0.486 and 0.497 for two regulated voltages.

6.1.3 Mode 3: In this mode, the test system has been further simulated for two subcases as PV power injection with and without reactive power support from PV inverter. Allocation of PV system in the network has been chosen based on the lowest node voltage profile. The lowest voltage has been observed at node 65 as shown in Table 3. Therefore, a residential PV system with 200 KVA rating of the smart inverter has been placed at node 65. The simulated results are depicted in fourth column of Table 3. It can be observed

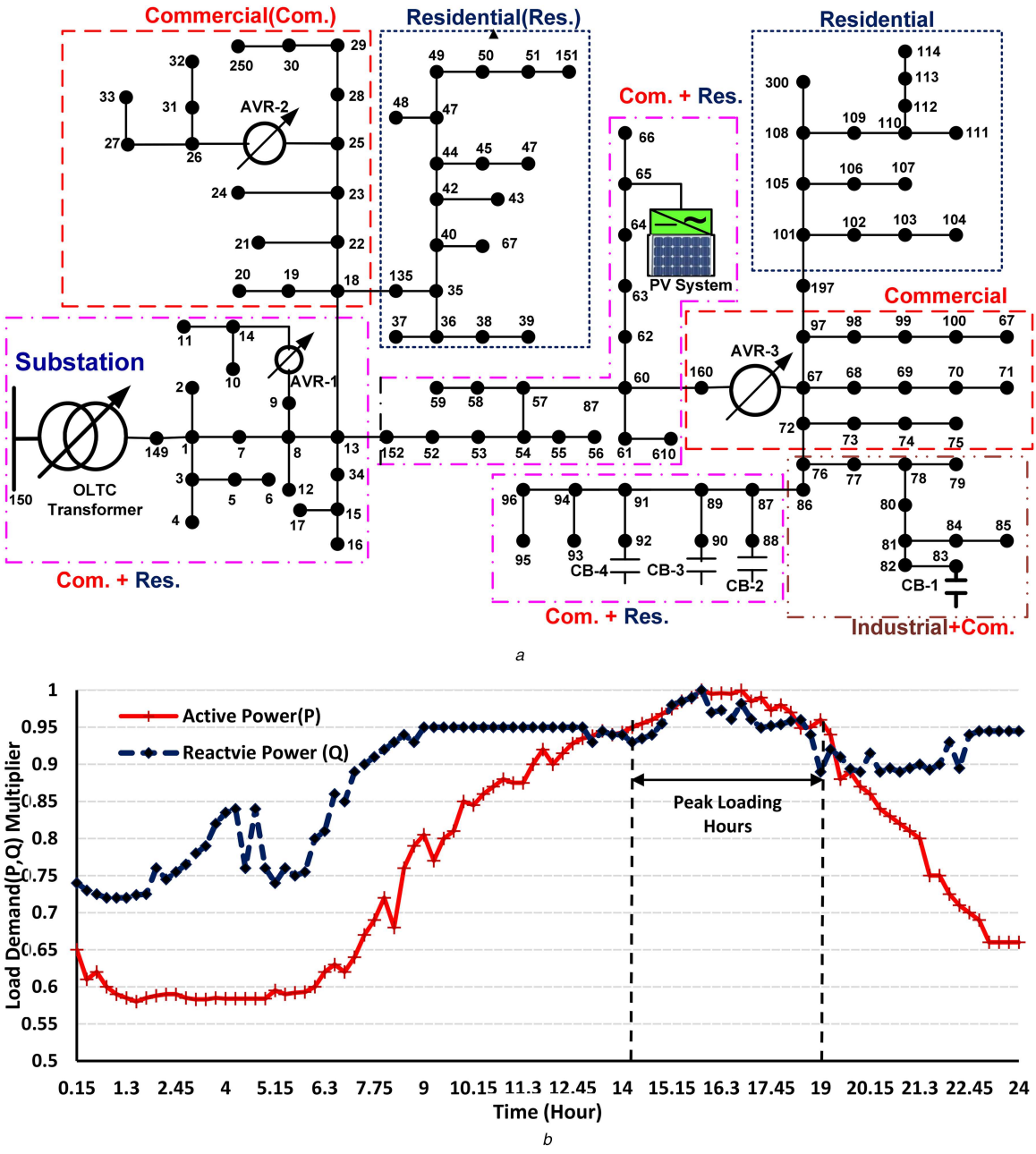

Fig. 5 *Test system and its load profile of a day*
(a) Modified IEEE 123 node distribution test feeder, ***(b)*** Load demand profile for 24 h

Table 1 Ratings and parameters of VVC devices

Device	Phase (Ph)/connection	Location at/between node/rating		Tap range/CB step per phase/inverter S_{max}	Maximum daily tap change/CB switching operation per phase
OLTC	3-Ph (a-b-c), Wye	150–149		+16 to −16	5
AVR-1	1-Ph, a	9–14		+16 to −16	5
AVR-2	2-Ph, a, c	25–26		+16 to −16	5
AVR-3	3-Ph, a, b, c	160–67		+16 to −16	5
CB-1(KVAR)	3-Ph, a-b-c	83	200/phase	0–4	3
CB-2(KVAR)	1-Ph, a	88	50/phase	0–1	3
CB-3(KVAR)	1-Ph, b	90	50/phase	0–1	3
CB-4(KVAR)	1-Ph, c	92	50/phase	0–1	3
PV inverter KVA	3-Ph, a-b-c	65	200	200	—
efficiency (η_{inv})	0.985 (when it is injecting either *P* or *Q* only) 0.97 (when it is injecting both *P* and *Q* simultaneously)				
VV droop characteristics points	point P1 voltage ($V_1^{P_1}$) = 0.945 pu and point P2 voltage ($V_2^{P_2}$) = 0.95 pu point P3 voltage ($V_3^{P_3}$) = 1.05 pu and Point P4 voltage ($V_4^{P_4}$) = 1.06 pu DB range = between points P2 and P3, 0.1 pu				

Table 2 ZIP load model parameters

Loading type	ZIP coefficients [7]		Node number
residential	$Z_p = 0.85$	$Z_q = 10.96$	2,4,5,6,7,10,12,16,35,37,38,39,41,42,43,45,46,47,48,49,50,51,52,53,55,56,58,59,60,65 94,95,96,102,103,104,106,107,109,111,112,113,114
	$I_p = -1.12$	$I_q = -18.73$	
	$P_p = 1.27$	$P_q = 8.77$	
large commercial	$Z_p = 0.4$	$Z_q = 4.06$	62,63,64, 66,80,82,85
	$I_p = -0.06$	$I_q = -6.65$	
	$P_p = 0.63$	$P_q = 3.59$	
small commercial	$Z_p = 0.85$	$Z_q = 4.06$	1,9,11,17,19,20,22,24,28, 29,30,31,32,33,34,68,69,70,71,73,74,75,83,84,87,88, 90,92,98,99,100
	$I_p = -1.12$	$I_q = -6.65$	
	$P_p = 1.27$	$P_q = 3.59$	
industrial	Z_p, $I_p = 0$, $P_p = 1$	Z_q, $I_q = 0$, $P_q = 1$	76,77,79,86

Table 3 Simulation results of Case I (peak demand reduction)

Energy (E) terms[a]	Mode 1	Mode 2		Mode 3	
	Without CVR	Only CVR		CVR with PV (117 V)	
	(124 V)	(119 V)	(117 V)	Without Q support	With Q support
$E_{consumption}$, MWh	17.747	17.400	17.248	16.845	16.842
energy losses, MWh (%)	0.446	0.460	0.467	0.449	0.4440
	(2.51)	(2.59)	(2.63)	(2.530)	(2.501)
E_{saving}, kWh (%)	—	347	499	901.7	904.417
		(+1.96)	(+2.81)	(+5.08)	(+5.09)
ΔE_{losses}, kWh (%)	—	+14	+21	−3.244	+1.840
		(+03.2)	(+4.7)	(+0.72)	(–0.41)
lowest voltage, pu, (node)	1.00	0.9634	0.9441	0.9464	0.9500
	(65)	(65)	(65)	(65)	(63)
CVR factor (CVR_{fE})	—	0.486	0.497	0.900	0.903

[a] $E_{consumption}$ - Energy Consumption, ΔE_{losses} - Change in energy losses.

from the table that about 5.08% reduction in energy demand is achieved during CVR with PV without Q support. However, the minimum voltage limit violated during time span 15:15–19:00 as shown in Fig. 6*b*. VVC operation with CVR and PV with Q support mode reported 5.09% reduced energy demand and 0.41% reduction in energy losses maintaining voltage profile within ANSI range. Fig. 6*b* clearly demonstrates the improvement in voltage under this mode of operation. The additional reactive power support is controlled by VV droop characteristics as shown in Fig. 2*a*. The droop characteristics assist in determining the appropriate amount of reactive power to be injected from the inverter to maintain the voltage within desired range. In the present case, droop control operation has been carried out in the range prior to point P_3 of droop characteristics. Since range between points P_2 and P_3 is DB range, the inverter starts injecting the reactive power prior to point P_2 (i.e. voltage below 0.95 pu) until desired reactive power is injected. Fig. 6*c* shows the active and reactive powers fed by PV system as well as its droop control. Active power losses and inverter losses are shown in Fig. 6*d* for this mode. From Fig. 6*d*, it is observed that inverter losses increased when it injected the reactive power (excluding time span 14:15–15:00 because during this time span, Q support is zero). However, increased inverter losses due to Q support does not affect the net system active power losses. The CVR_{fE} for subcases without and with reactive power support have been found to be 0.900 and 0.903, respectively, as shown in Table 3.

It can be comprehended from the aforesaid results that the maximum peak demand reduction would be achieved by application of CVR with PV system extending the reactive power support. The CVR factor estimated in this work measures the effectiveness of deployment of CVR. This factor also indicates that operation in Mode 3 performed better than Mode 2.

6.2 Case II – daily energy demand reduction or daily energy savings

In this case study, CVR scheme is tested with the aim of reduction in daily energy demand. The proposed scheme is deployed on the same system for a maximum demand day of a week. Entire day's load profile of the day as shown in Fig. 5*b* has again been used to demonstrate the effect of all the three modes of VVC operation. The simulated results related to energy consumption and losses are shown in Table 4. Total active power demand and lowest node voltage profile during whole day operation are shown in Figs. 7*a* and *b*, respectively. The obtained simulation results from each mode are discussed as under.

6.2.1 Mode 1: The simulation results during without CVR operation is obtained with the execution of VVC at 124 V regulated voltage. Table 4 shows the total active energy demand and active power losses. Fig. 7*a* shows the active power demand of the system for the considered duration.

6.2.2 Mode 2: The test system has been simulated for two regulated voltages of 119 and 117 V as shown in Table 4. From results, it can be demonstrated that during CVR, a significant energy savings amounting 1.9 and 2.83% are achieved. However, the energy losses have been increased to 2.85 and 4.08%. The increased losses are included in achieved total energy savings. From Fig. 7*b*, it is observed that the minimum voltage limit is violated at some nodes of the feeder end during CVR operation at 117 V. The values of CVR_{fE} are 0.47 and 0.50, respectively, for two regulated voltages.

6.2.3 Mode 3: In this mode, the test system is simulated with CVR and PV at 117 V regulated voltage with and without reactive power supports. The energy savings in this mode is increased to 4.727% and losses are almost equal to the Mode 1. The feeder

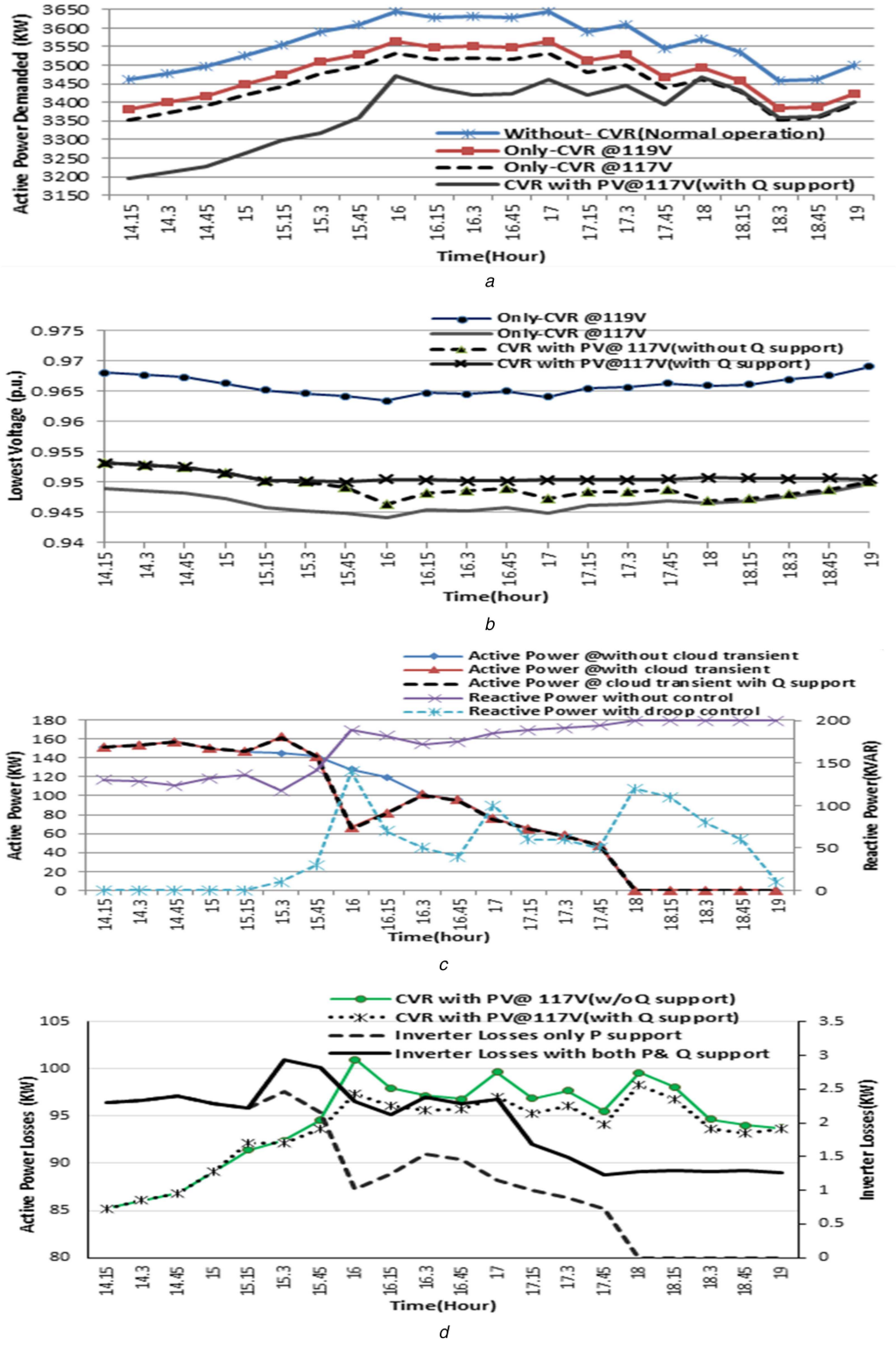

Fig. 6 *Simulation results of test case I (peak demand hours)*

(a) Active power demand at feeder head in all modes of operations, ***(b)*** Minimum node voltage profile in all modes of operations, ***(c)*** *P* and *Q* power feeds by PV system during Mode 3 operation, ***(d)*** Active power losses and inverter losses during Mode 3 operation

voltage profile is maintained within limits with the injection of PV power during CVR operation at 117 V as shown in Fig. 7*b*. The power loss variation throughout the day has been shown in Fig. 7*c*. The PV power profile during the entire day is shown in Fig. 7*d*. The calculated $CVR_{/E}$is 0.89 which is higher than Mode 2.

Entire day tap positions of OLTC and AVRs are shown in Figs. 8*a–d*. It is observed that tap positions have been reduced with the enabling of CVR. Per phase tap operations for the day for every device are limited to the maximum five times which are clearly portrayed in Figs. 8*a–d* also. The CB switching operations for the day are also restricted up to three times per phase and it has been shown in Table 5.

From above-discussed case studies, it is demonstrated that considerable energy consumptions and peak power demand can be reduced with CVR operation. To achieve higher-energy savings through deeper CVR operation is not the secure way. Therefore, deployment of CVR scheme with PV system is advisable.

Table 4 Simulation results of Case II (whole day operation)

Energy (E) terms	Mode 1 Without CVR (124 V)	Mode 2 Only CVR (119 V)	Mode 2 Only CVR (117 V)	Mode 3 CVR with PV (117 V) Without Q support	Mode 3 CVR with PV (117 V) With Q support
$E_{consumption}$, MWh	68.159	66.863	66.232	64.9397	64.9370
energy losses, MWh (%)	1.469	1.511	1.5292	1.4783	1.4732
	(2.15)	(2.21)	(2.24)	(2.168)	(2.161)
E_{saving}, MWh (%)	—	1.30	1.93	3.2192	3.2219
		(+1.90)	(+2.83)	(+4.724)	(+4.727)
ΔE_{losses}, kWh (%)	—	42	+60.2	+9.098	+4.08
		(+2.85)	(+4.08)	(+0.61)	(+0.272)
lowest voltage, pu, (node)	1.00	0.9634	0.9441	0.9464	0.9500
	(65)	(65)	(65)	(65)	(63)
CVR factor (CVR_{fE})	—	0.47	0.50	0.8366	0.8374

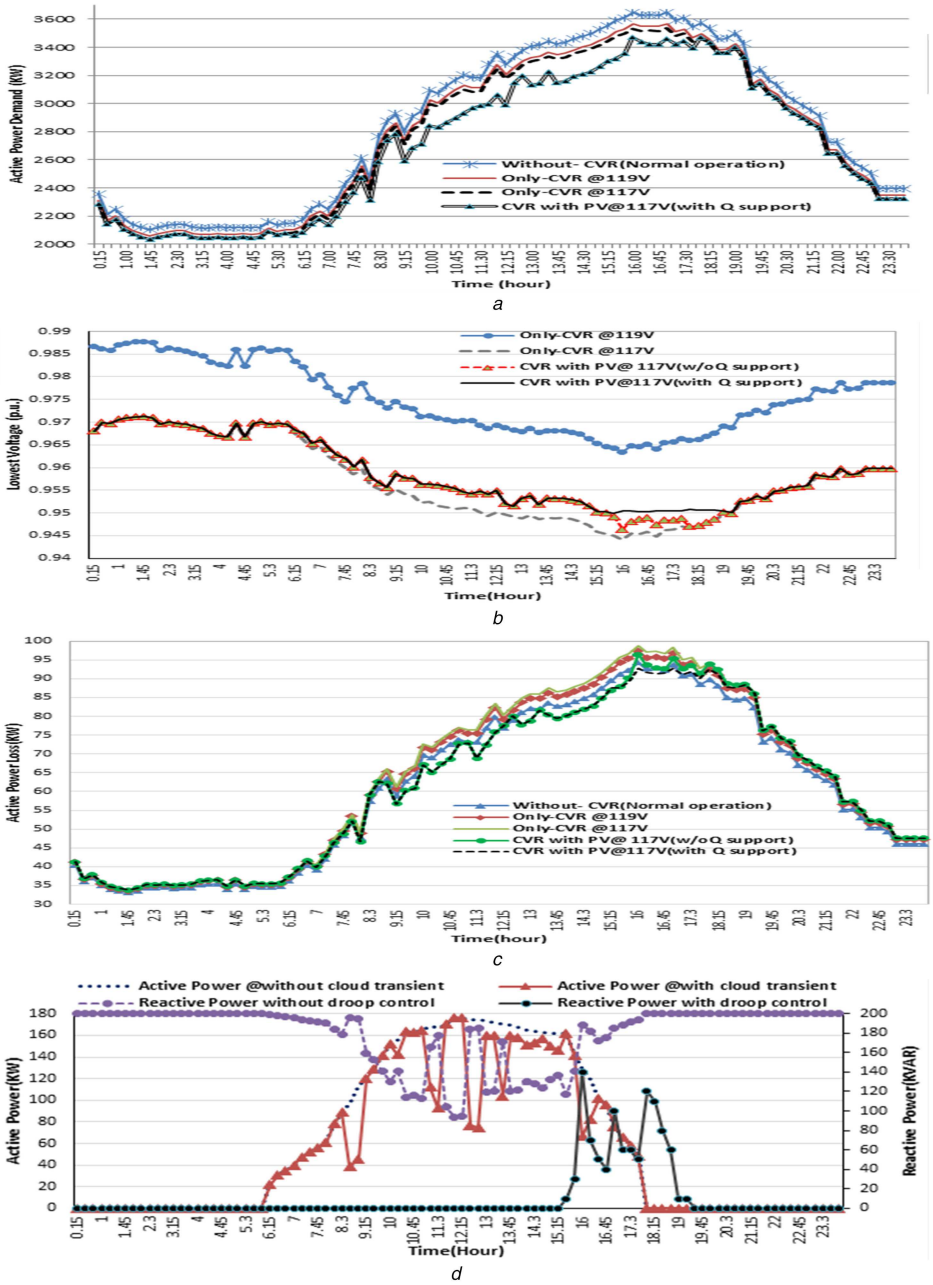

Fig. 7 *Simulation results of test case II (whole day operation)*
(a) Active power demand at feeder head in all modes of operations, ***(b)*** Minimum node voltage profile, ***(c)*** Active power losses in all modes of operations, ***(d)*** P and Q power feeds by PV system during Mode 3 operation

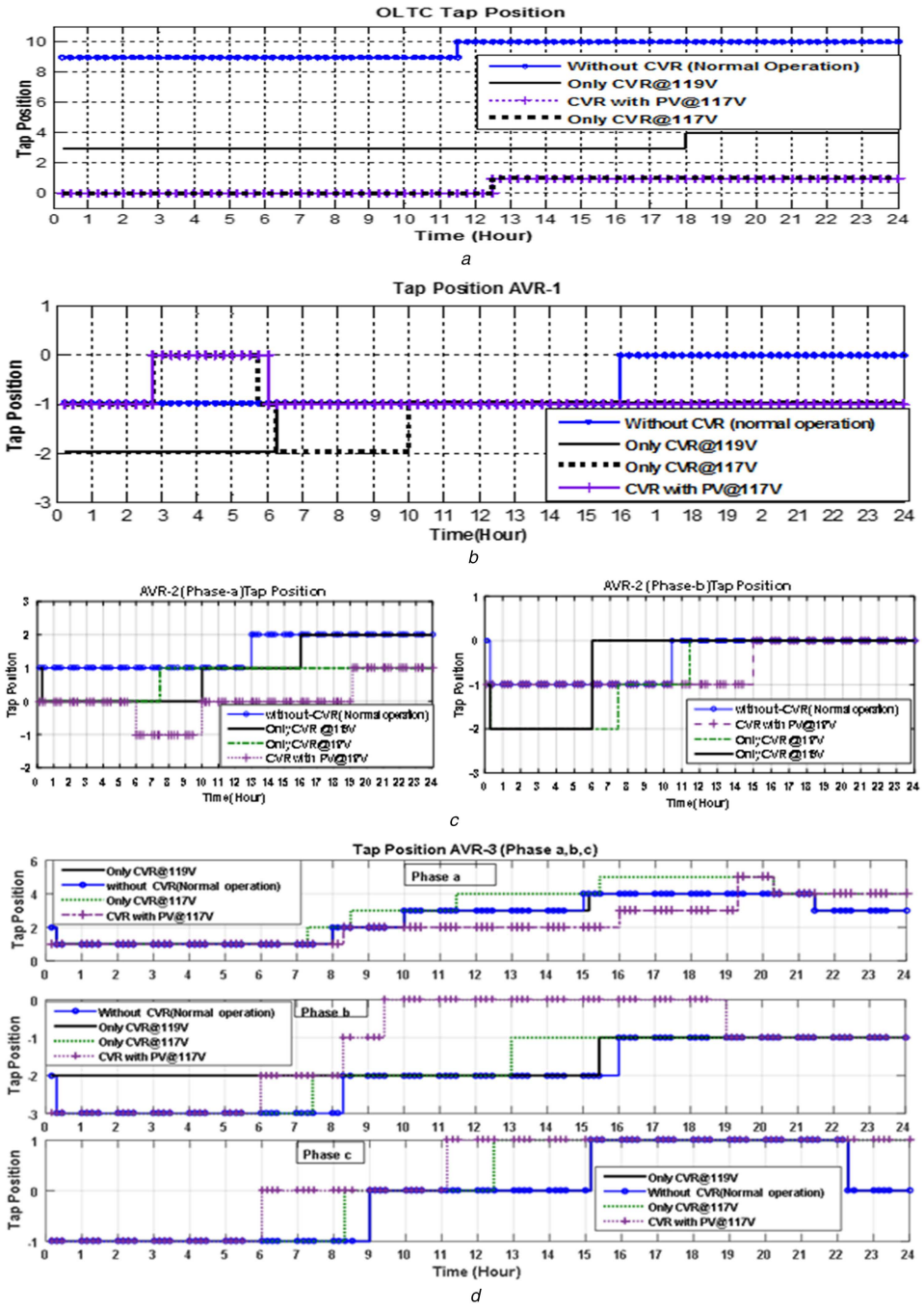

Fig. 8 *Tap positions of*
(a) OLTC, ***(b)*** AVR-1, ***(c)*** AVR-2, ***(d)*** AVR-3 for whole day operation

Table 5 Capacitor banks switching status

Mode		Mode 1	Mode 2		Mode 2		Mode 3	
		Without CVR	Only CVR (119 V)		Only CVR (119 V)		CVR with PV (117 V)	
Time duration		00:24	00.15–6.00	6.15–24.00	00.15–6.00	6.15–24.00	00.15–6.00	6.15–24.00
CB-1	Phase-a	4	2	3	2	3	2	3
	Phase-b	4	2	2	2	2	2	2
	Phase-c	4	2	3	2	3	2	3
CB-2		1	0	1	0	1	0	1
CB-3		1	0	1	0	1	0	1
CB-4		1	0	1	0	1	0	1

6.3 Moving cloud effect

The partial clouds affect the output of the PV system. The effect of partial cloudy day on the power output of PV system under Mode 3 operation has also been studied in both the cases. Figs. 6*c* and 7*d* exhibit the active and reactive powers supplied by the system in Case 1 and Case 2, respectively. It can very well be noted from these figures that power output is fluctuating in nature because of movement of clouds on PV arrays. The sudden fall in PV power output followed by a rise in power output indicate the interventions of cloud and its disappearance. Consequently, the voltage rise/fall and reversible power flow problem may occur during PV

penetrations. This can be mitigated if the PV system operates in association with CVR. Lower-level PV penetrations are the best solutions for handling the fluctuation in PV power output; otherwise, PV system needs to be equipped with energy storage.

7 Conclusion

This paper has analysed the effect of smart grid-enabled CVR with the cooperation of solar PV inverter on energy demand. VVC operation has been carried out without and with smart grid-enabled CVR to estimate the energy savings. Findings of this investigation are as under:

- Significant energy savings and peak loading relief have been achieved with only CVR.
- The higher-energy savings have been achieved with CVR and solar PV system during deeper level voltage reduction within voltage regulatory range.
- The PV inverter injects the droop-controlled reactive power within limits during lower-voltage limit violation.
- The effect of inverter losses during reactive power support has also been analysed.
- Moving clouds effect on with PV power output has been analysed.

It can be concluded that the CVR operation with PV system yields the higher reduction in energy consumptions, peak load demand, and system losses within ANSI voltage range in comparison with only CVR.

8 References

[1] Farhangi, H.: 'A road map to integration: perspective on smart grid development', *IEEE Power Energy Mag.*, 2014, **12**, (3), pp. 52–66

[2] ANSI C84.1-1995: 'American national standards for electric power systems and equipment – voltage ratings (60 Hz)', 1995

[3] Zhaoyu, W., Jianhui, W.: 'Review on implementation and assessment of conservation voltage reduction', *IEEE Trans. Power Syst.*, 2014, **29**, (3), pp. 1306–1315

[4] Diskin, E., Fallon, T., Mahony, G.O., *et al.*: 'Conservation voltage reduction and voltage optimisation on Irish distribution networks'. Proc. Int. Conf. Integration of Renewables into the Distribution Grid, 2012, pp. 1–4

[5] Ellens, W., Berry, A., West, S.: 'A quantification of the energy savings by conservation voltage reduction'. Proc. Int. IEEE Conf. Power System Technology, 2012, pp. 1–6

[6] Schneider, F.K., Tuffner, F., Singh, R.: 'Evaluation of conservation voltage reduction (CVR) on a national level'. Available at http://www.pnl.gov/main/publications/external/technical_reports/PNNL-19596.pdf, accessed July 2015

[7] Diaz-Aguiló, M., Sandraz, J., Macwan, R., *et al.*: 'Field validated load model for the analysis of CVR in distribution secondary networks: energy conservation', *IEEE Trans. Power Deliv.*, 2013, **28**, pp. 2428–2436

[8] Chanda, S., Shariatzadeh, F., Srivastava, A., *et al.*: 'Implementation of non-intrusive energy saving estimation for volt/VAr control of smart distribution system', *Electr. Power Syst. Res.*, 2015, **120**, pp. 39–46

[9] Padilha-Feltrin, A., Rodezno, D.A.Q., Mantovani, J.R.S.: 'Volt-VAR multiobjective optimization to peak-load relief and energy efficiency in distribution networks', *IEEE Trans. Power Deliv.*, 2015, **30**, (2), pp. 618–626

[10] Milosevic, B., Begovic, M.: 'Capacitor placement for conservative voltage reduction on distribution feeders', *IEEE Trans. Power Deliv.*, 2004, **9**, (2), pp. 1360–1367

[11] Singh, S., Shukla, D., Singh, S.P.: 'Peak demand reduction in distribution network with smart grid-enabled CVR'. Proc. IEEE Innovative Smart Grid Technologies, Melbourne, VIC, 2016, pp. 735–740

[12] Shivarudraswamy, R., Gaonkar, D.N.: 'Coordinated voltage control using multiple regulators in distribution system with distributed generators', *World Acad. Sci. Eng. Technol.*, 2011, **74**, pp. 574–578

[13] Bokhari, A., Raza, A., Diaz-Aguiló, M., *et al.*: 'Combined effect of CVR and DG penetration in the voltage profile of low-voltage secondary distribution networks', *IEEE Trans. Power Deliv.*, 2016, **31**, (1), pp. 286–293

[14] Quijano, D.A, Feltrin, A.P.: 'Assessment of conservation voltage reduction effects in networks with distributed generators'. Proc. IEEE PES Innovative Smart Grid Technologies, Montevideo, Latin America, 2015, pp. 393–398

[15] Singh, R., Tuffner, F., Fuller, J., *et al.*: 'Effects of distributed energy resources on conservation voltage reduction (CVR)'. Proc. IEEE PES General Meeting, San Diego, CA, July 2011, pp. 24–29

[16] Divoiu, C., Gheorghe, I.G.: 'Methods for reactive power compensation in photovoltaic parks', *Rom. Rev. Prec. Mech. Opt. Mechatronics*, 2015, **48**, pp. 273–275

[17] Cagnano, A., De Tuglie, E.: 'A decentralized voltage controller involving PV generators based on Lyapunov theory', *Renew. Energy*, 2016, **86**, pp. 664–674

[18] Kabir, M.N., Mishra, Y., Ledwich, G., *et al.*: 'Coordinated control of grid-connected photovoltaic reactive power and battery energy storage systems to improve the voltage profile of a residential distribution feeder', *IEEE Trans. Ind. Inf.*, 2014, **10**, (2), pp. 967–977

[19] Jahangiri, P., Dionysios, C.A.: 'Distributed volt/VAr control by PV inverters', *IEEE Trans. Power Syst.*, 2013, **28**, (3), pp. 3429–3439

[20] Juamperez, M., Yang, G., Kjaer, S.B., *et al.*: 'Voltage regulation in LV grids by coordinated volt-var control strategies', *J. Mod. Power Syst. Clean Energy*, 2014, **2**, (4), pp. 319–328

[21] Smith, J.W., Sunderman, W., Dugan, R., *et al.*: 'Smart inverter volt/var control functions for high penetration of PV on distribution systems'. Proc. IEEE/PES Power Systems Conf. Exposition, 2011

[22] Bahramipanah, M., Cherkaoui, R., Paolone, M.: 'Decentralized voltage control of clustered active distribution network by means of energy storage systems', *Electr. Power Syst. Res.*, 2016, **136**, pp. 370–382

[23] Calderaro, V., Conio, G., Galdi, V., *et al.*: 'Optimal decentralized voltage control for distribution systems with inverter-based distributed generators', *IEEE Trans. Power Syst.*, 2014, **29**, (1), pp. 230–241

[24] Farivar, M., Clarke, C.R., Low, S.H., *et al.*: 'Inverter VAR control for distribution systems with renewables'. Proc. IEEE Int. Conf. Smart Grid Communications, Brussels, 2011, pp. 457–462

[25] Liu, H.J.: 'Smart-grid-enabled distributed reactive power support with conservation of voltage reduction'. Master thesis, University of Illinois at Urbana-Champaign, 2013

[26] Singh, S., Thakur, A.K., Singh, S.P.: 'Energy savings in distribution network with smart grid-enabled CVR and distributed generation'. National Power System Conf., Bhubaneswar, 19–21 December 2016, pp. 1–6

[27] Dao, T.V., Chaitusaney, S., Nguyen, H.T.N.: 'Linear least-squares method for conservation voltage reduction in distribution systems with photovoltaic inverters', *IEEE Trans. Smart Grid*, 2015, **99**, pp. 1–12

[28] Kersting, W.H.: '*Distribution system modeling and analysis*' (CRC Press, New York, NY, 2007)

[29] Singh, G.D., Singh, S.P., Raju, G.S., *et al.*: 'Methodology for alleviation of voltage excursions in large power systems', *Int. J. Electr. Power Energy Syst.*, 1996, **18**, (3), pp. 167–173

[30] 'IEEE PES distribution test feeders'. Available at http://www.ewh.ieee.org/soc/pes/dsacom/testfeeders, accessed July 2016

[31] Electric Power Research Institute: 'OpenDSS Manual', July 2010